Cystic Fibrosis Is Associated with a Defect in Apical Receptor–Mediated Endocytosis in Mouse and Human Kidney

François Jouret,* Alfred Bernard,† Cédric Hermans,‡ Geneviève Dom,§ Sara Terryn,‖ Teresinha Leal,¶ Patrick Lebecque,** Jean-Jacques Cassiman,†† Bob J. Scholte,‡‡ Hugo R. de Jonge,‡‡ Pierre J. Courtoy,§ and Olivier Devuyst*

*Division of Nephrology, †Department of Public Health, Unit of Industrial Toxicology and Occupational Medicine, ‡Haemostasis and Thrombosis Unit, §Christian de Duve Institute of Cellular Pathology, Cell Unit, ¶Department of Clinical Chemistry, and **Department of Pneumology–Paediatrics, Université catholique de Louvain, Brussels, ‖Laboratory of Cell Physiology, Centrum voor Milieukunde, Universiteit Hasselt, Diepenbeek, and ††Center for Human Genetics, University of Leuven, Leuven, Belgium; and ‡‡Departments of Biochemistry/Cell Biology, Erasmus University Medical Center, Rotterdam, The Netherlands

Inactivation of the chloride channel cystic fibrosis transmembrane conductance regulator (CFTR) causes cystic fibrosis (CF). Although CFTR is expressed in the kidney, no overwhelming renal phenotype has been documented in patients with CF. This study investigated the expression, subcellular distribution, and processing of CFTR in the kidney; used various mouse models to assess the role of CFTR in proximal tubule (PT) endocytosis; and tested the relevance of these findings in patients with CF. The level of CFTR mRNA in mouse kidney approached that found in lung. CFTR was located in the apical area of PT cells, with a maximal intensity in the straight part (S3) of the PT. Fractionation showed that CFTR co-distributed with the chloride/proton exchanger ClC-5 in PT endosomes. *Cftr*$^{-/-}$ mice showed impaired ^{125}I-β_2-microglobulin uptake, together with a decreased amount of the multiligand receptor cubilin in the S3 segment and a significant loss of cubilin and its low molecular weight (LMW) ligands into the urine. Defective receptor-mediated endocytosis was found less consistently in *Cftr*$^{\Delta F/\Delta F}$ mice, characterized by a large phenotypic heterogeneity and moderate *versus* mice that lacked ClC-5. A significant LMW proteinuria (and particularly transferrinuria) also was documented in a cohort of patients with CF but not in patients with asthma and chronic lung inflammation. In conclusion, CFTR inactivation leads to a moderate defect in receptor-mediated PT endocytosis, associated with a cubilin defect and a significant LMW proteinuria in mouse and human. The magnitude of the endocytosis defect that is caused by CFTR *versus* ClC-5 loss likely reflects functional heterogeneity along the PT.

J Am Soc Nephrol 18: 707–718, 2007. doi: 10.1681/ASN.2006030269

Cystic fibrosis (CF; MIM #219700), the most common autosomal recessive disease in white individuals, is caused by mutations in the *CFTR* gene that encodes the chloride channel cystic fibrosis transmembrane conductance regulator (CFTR) (1,2). CFTR is a 1480–amino acid protein that belongs to the ATP-binding cassette (ABC) family of integral membrane proteins. It is located mainly in the apical membrane area of secretory epithelia, where it functions as a cAMP-dependent chloride channel and as a conductance regulator *via* interactions with other ion channels (2). Mutations in *CFTR* are classified into five groups according to their structural or functional consequences on the protein. The deletion of three bases that encode a phenylalanine residue at position 508 (ΔF508), which occurs in approximately 70% of patients with CF, results in the misfolding and lack of maturation of the CFTR protein (3). Most of the clinical features that are observed in patients with CF and CF mouse models originate from mucosal obstruction of exocrine glands, such as the respiratory system, pancreas, intestine, gallbladder, and sweat glands (1–3).

Besides exocrine epithelia, CFTR has been located in the mammalian kidney, which primarily ensures reabsorptive functions (4). During human nephrogenesis, CFTR is expressed in the apical membrane of the branching ureteric bud and, later, in the apical pole of proximal tubule (PT) cells in the cortex, where it remains detected after birth (5,6). A functional truncated isoform also has been described in the kidney, with a distinct ontogeny pattern and a minor plasma membrane expression (7,8). Despite the high level of CFTR expression in the developing and mature kidney, no overwhelming renal phenotype has been associated with CF (4,9). Instead, a spectrum of renal diseases is apparent from the neonatal period to later in life. Microscopic nephrocalcinosis has been reported in an autopsy series of patients who had CF and ranged in age from birth to 36 yr (10), and the incidence of kidney stones in patients

Received March 24, 2006. Accepted December 17, 2006.

Published online ahead of print. Publication date available at www.jasn.org.

Address correspondence to: Dr. Olivier Devuyst, Division of Nephrology, Université catholique de Louvain, 10 Avenue Hippocrate, B-1200 Brussels, Belgium. Phone: +32-2-764-54-53; Fax: +32-2-764-54-55; E-mail: devuyst@nefr.ucl.ac.be

ISSN: 1046-6673/1803-0707

with CF also may be increased (11). However, the relative contribution of lithogenic factors, such as hypocitraturia, or impaired hydration remains elusive. A decreased capacity to dilute urine, together with reduced urinary sodium excretion, also has been reported in patients with CF (12). This could result from a primary defect in kidney function or simply reflect changes in the extracellular fluid volume that is caused by excessive losses of NaCl in sweat and feces. In addition, patients with CF show an enhanced renal clearance of many drugs, including aminoglycosides (13), and subtle abnormalities in kidney development, function, and/or morphology may appear in later stages of CF (6).

In addition to its location in the apical membrane, CFTR is distributed in intracellular organelles along the endocytic and secretory pathways (14,15). Inhibition of endocytic activity, as well as defective acidification in *trans*-Golgi and prelysosomal compartments, has been reported in CF cells (16). However, the exact role of CFTR in regulating organelle pH remains controversial, with hyper- rather than hypo-acidification suggested to occur in CF respiratory epithelial cells (17). Recent findings about the endosomal protein ClC-5, which belongs to the CLC family of Cl^- channels/exchangers, have provided insights into the role of anion transporters in PT cells (18). In normal conditions, low molecular weight (LMW) proteins as well as albumin and transferrin in some species are ultrafiltered by the glomerular membrane but almost entirely reabsorbed by receptor-mediated endocytosis at the apical side of PT cells (19). The loss of ClC-5, which co-distributes with the vacuolar H^+-ATPase (V-ATPase) in PT endosomes, causes a major defect in receptor-mediated endocytosis and an LMW proteinuria in *Clcn5* knockout (KO) mice (20,21) as in patients with Dent's disease, which is caused by inactivating mutations in *CLCN5* (22). By analogy, other intracellular anionic transporters such as CFTR might play a role in the endocytic reabsorption of LMW proteins by the kidney (4,18).

In this study, we describe the segmental and subcellular distribution of CFTR in the kidney, at both the mRNA and protein levels. Taking advantage of $Cftr^{-/-}$ and $Cftr^{\Delta F/\Delta F}$ mutant mice, we characterize the role of CFTR in PT apical endocytosis, in comparison with the $Clcn5^{Y/-}$ mouse model. Finally, we evaluate the renal handling of LMW proteins in cohorts of patients who have CF and harbor the ΔF508 mutation and patients with chronic lung inflammation as a result of asthma, each compared with age- and gender-matched control subjects.

Materials and Methods

CF Mouse Models

Experiments were conducted on 12-wk-old, gender-matched $Cftr^{+/+}$ and $Cftr^{-/-}$ mice (129/C57BL/6 background), generated by targeted deletion of exon 10 of *Cftr* (23), and gender-matched $Cftr^{N/N}$ and mutated $Cftr^{\Delta F/\Delta F}$ mice (FVB background), generated by double homologous recombination (24). All mice had free access to appropriate standard diet (Carfil Quality, Oud-Turnhout, Belgium). Tap water of mice with CF was enriched with Kleanprep solution (Helsinn Birex Pharmaceuticals, Dublin, Ireland). The renal phenotype of mice with CF was compared with $Clcn5^{Y/-}$ mice, an established model of Dent's disease (21,25). The experiments were conducted in accordance with the National Institutes of Health Guide for the Care and Use of Laboratory Animals and were approved by the Ethics Committee of the Université catholique de Louvain.

Microdissection Studies

Kidneys from male C57BL/6 mice were dissected and minced before incubation with 0.1% (wt/vol) type 2 collagenase solution that contained 100 μg/ml soybean trypsin inhibitor for 30 min at 37°C. After digestion, the supernatant was sieved through 250- and 80-μm nylon filters. Nephron fragments remained in the 80-μm sieve and were resuspended by flushing. Distinct segments (glomeruli, S1 and S3 PT, thick ascending limbs [TAL], and inner medullary collecting ducts [IMCD]) were isolated upon their morphologic features (26) and preserved in RNA later (Westburgh, Leusden, The Netherlands). Four distinct collections were snap-frozen in liquid nitrogen and conserved at −80°C. The extraction of total RNA was performed using RNAqueous-Micro (Ambion, Huntingdon, UK).

Real-Time Reverse Transcriptase–PCR Analyses

Total RNA from mouse kidney samples was extracted by Trizol (Invitrogen, Merelbeke, Belgium), treated with DNase I (Invitrogen), and reverse-transcribed into cDNA using SuperScript II Rnase H (Invitrogen). Specific mouse primers were designed using Beacon Designer 2.0 (Premier Biosoft International, Palo Alto, CA; see Supplementary Table 1). Real-time reverse transcriptase–PCR (RT-PCR) analyses were performed in duplicate with 200 nM of both sense and antisense primers in a final volume of 25 μl of iQ SYBR Green Supermix (Bio-Rad, Nazareth, Belgium). The PCR mixture contained 10 nM fluorescein for initial well-to-well fluorescence normalization. PCR conditions were settled as incubation at 94°C for 3 min followed by 40 cycles of 30 s at 95°C, 30 s at 61°C, and 1 min at 72°C. The melting temperature of PCR product was checked at the end of each PCR by recording SYBR green fluorescence increase upon slowly renaturing DNA. For each assay, standard curves were prepared by serial four-fold dilutions of mouse adult kidney cDNA, and primer efficiencies were calculated [efficiency = $(10^{-1/\text{slope}}) - 1$] (Supplementary Table 1). CFTR mRNA expression was investigated in four adult male lungs and kidneys, after normalization to HPRT1: Ratio = $2^{\Delta Ct\ (Lung\ -\ Kidney)\ CFTR}/2^{\Delta Ct\ (Lung\ -\ Kidney)HPRT1}$. CFTR mRNA expression was quantified further in S1 *versus* S3 PT samples: Ratio = $2^{\Delta Ct\ (GAPDH\ -\ CFTR)}$. Real-time PCR results were confirmed with two sets of primers for CFTR and ClC-5 and using two reporter genes, *HPRT1* and *GAPDH*.

Antibodies

The following antibodies were used: Affinity-purified rabbit polyclonal antibodies (MD1314) against the C-terminus of rodent CFTR (27) (Dr. C.R. Marino, VA Medical Center, University of Tennessee, Memphis, TN), the N-terminus of human ClC-5 (21), aquaporin-1 (AQP1; Chemicon, Temecula, CA), cubilin (Dr. P. Verroust, INSERM, Paris, France), Rab5a (Santa Cruz Biotechnology, Santa Cruz, CA), villin (Dr. D. Louvard and S. Robine, Institut Curie, Paris, France), and transferrin (Dako, Glostrup, Denmark); goat polyclonal antibodies against cathepsin D (Santa Cruz Biotechnology); sheep polyclonal antibodies against megalin (Dr. P. Verroust); mouse monoclonal antibodies (E11) against the E1 subunit of V-ATPase (Dr. S. Gluck, University of California, San Francisco, CA) and β-actin (Sigma, St Louis, MO).

Western Blotting and Deglycosylation Studies

Membrane extracts were prepared as described previously (28). Kidney samples were homogenized in ice-cold sucrose buffer that contained Complete protease inhibitors (Roche, Vilvoorde, Belgium) and centrifuged at 1000 × *g* for 15 min at 4°C. The supernatant was

centrifuged at 100,000 × *g* for 120 min at 4°C. The resulting pellet ("membrane" fraction) was suspended in ice-cold homogenization buffer and stored at −80°C. Protein concentrations were determined with the bicinchoninic acid protein assay using BSA as standard. Deglycosylation studies using N-glycosidase F and endoglycosidase H (Roche) were performed following the manufacturer's recommendations. Equal loading was verified by reprobing against β-actin. All immunoblots were performed at least in duplicate.

Immunostaining

Kidney samples were fixed in 4% formaldehyde (Boehringer Ingelheim, Heidelberg, Germany) in 0.1 M phosphate buffer (pH 7.4), before embedding in paraffin as described (28). Six-micrometer sections first were incubated in 0.01 M citrate buffer (pH 5.8) for 75 min in a water bath heated at 97°C before cooling and rinsing. After endogenous peroxidase was blocked for 30 min with 0.3% hydrogen peroxide, sections were incubated with 10% normal serum, then with the primary antibodies diluted in PBS that contained 2% BSA. After washing, sections were incubated successively with biotinylated secondary anti-IgG antibodies, avidin-biotin peroxidase, and aminoethylcarbazole (Vector Laboratories, Brussels, Belgium). For immunohistofluorescence, freshly collected kidneys were immersed in Tissue-Tek OCT compound (Sakura Finetek, Zoeterwoude, The Netherlands) and frozen at −80°C. Tissue sections (5 μm thick) were dried overnight at 37°C, fixed with ice-cold formaldehyde 4% for 10 min, washed with PBS, and processed for immunostaining. Secondary antibodies were goat anti-rabbit and donkey anti-sheep coupled to Alexa 488 (Molecular Probes, Merelbeke, Belgium). Sections were viewed under a Leica DMR coupled to a Leica DC300 digital camera (Leica, Heerbrugg, Switzerland).

Analytical Subcellular Fractionation

Kidneys were homogenized in 0.25 M sucrose and 3 mM imidazole buffer (pH 7.4) that contained Complete (Roche), in a Potter-Elvehjem tissue homogenizer (Thomas Scientific, Swedesboro, NJ) (29). A low-speed "nuclear" fraction was pelleted at 700 × *g* for 10 min and extracted twice by resuspension/sedimentation; pooled postnuclear supernatants were sedimented further at 100,000 × *g* for 60 min in a 50Ti fixed-angle rotor (Beckman, Palo Alto, CA). This high-speed pellet was resuspended in 1 ml of homogenization buffer, mixed with 7 ml of 16% (vol/vol) Percoll (average final density 1.048 g/ml), layered over a 250-μl Percoll cushion, and centrifuged at 60,000 × *g* for 30 min in a 50Ti rotor into a self-generating gradient. Ten fractions (750 μl each) were collected from the bottom and numbered from 1 (light) to 10 (dense).

Measurement of Endocytic Tracer Uptake

Mice were anesthetized under anesketin (Eurovet, Brussels, Belgium) and rompun (Bayer, Brussels, Belgium) and injected intravenously with 620 ng/g body wt radiolabeled ^{125}I-β_2-microglobulin (Sigma). After 7 min, kidneys were exsanguinated *in situ*. One kidney was fixed for 6 h at 4°C in 4% formaldehyde for further investigations, such as immunostaining and autoradiography. The contralateral kidney and the liver were homogenized and analyzed biochemically as previously reported (25).

Urine and Plasma Analyses

Mice were kept in metabolic cages for 24 h with *ad libitum* access to food and drinking water. Urine was collected on ice-cold Complete (Roche). Blood was obtained by aorta puncture at the time of killing. Plasma and urine levels of electrolytes, urea, and creatinine were measured by standard methods (Eastman Kodak Co., Rochester, NY), whereas CC16 concentration, a 16-kD marker for PT dysfunction, was determined in duplicate by latex immunoassay (21). Acid-base parameters in mouse urine and blood were determined using ABL 77 series apparatus (Radiometer, Copenhagen, Denmark).

Cohorts of Patients and Control Subjects

Two cohorts of patients were sampled for urinalyses. The first cohort included 30 patients with CF (range 3 to 39 yr of age) with their age- and gender-matched healthy control subjects. The diagnosis of CF was based on clinical characteristics and a positive sweat testing (3). Genotyping identified the ΔF508 mutation in all patients (homozygous in 25 of 30; heterozygous with N1303K, G542X, or 3849 10 kb CIIT in three of 30; second mutation not identified in two of 30). The second cohort included 25 patients with chronic active asthma (range 3 to 49 yr of age) and age- and gender-matched healthy control subjects. First-morning (CF cohort) or second-morning (asthma cohort) urine samples were analyzed for creatinine, albumin, CC16, β_2-microglobulin, transferrin (30,31), and calcium. Both cohorts were sampled during their routine follow-up at the St.-Luc Academic Hospital (Brussels, Belgium). The protocol was approved by the Université catholique de Louvain Ethical Review Board. All patients and control subjects gave informed consent.

Statistical Analyses

Unless specified otherwise, data are means ± SEM. Non-normally distributed parameters were compared after log transformation. Univariate analysis was performed using Pearson cross-product correlations. A multiple stepwise linear regression model was performed to assess the significant determinants of the urine protein ratios (age, gender, disease state, and previous aminoside treatment). All analyses were performed using SPSS V11.5.1 software (Chicago, IL).

Results

Expression and Distribution of CFTR mRNA and Protein in Mouse Kidney

Real-time RT-PCR analyses showed that the level of CFTR mRNA in adult mouse kidney reached approximately 60% of that found in lung, considered as reference organ (Figure 1A). The segmental distribution of CFTR mRNA in mouse nephron was investigated using tubular fractions that were obtained by microdissection. These fractions were characterized for segment-specific markers, such as podocin (glomeruli), AQP1 (PT), ClC-Kb (TAL), and AQP2 (IMCD; Figure 1B). The tissue-nonspecific alkaline phosphatase (tnAP) was approximately eight-fold enriched in samples from the convoluted (S1 to S2) part of the PT, allowing them to be distinguish from the straight descending (S3) PT segment (Figure 1C) (32). In these tubular fractions, CFTR mRNA was approximately three-fold more expressed in the straight S3 than in S1 to S2 PT fragments, in contrast with stable ClC-5 mRNA abundance (Figure 1C). Note that RT-PCR using three different sets of primers did not detect CFTR in glomeruli, TAL, and IMCD.

Immunoblotting demonstrated a distinct pattern for CFTR in mouse kidney and lung (Figure 1D). In lung samples, both the partially glycosylated precursor (B band at approximately 150 kD) and the fully glycosylated (C band at approximately 180 kD) CFTR were distinguished clearly. In the kidney, CFTR was detected as a single, approximately 160-kD band. Deglycosylation studies demonstrated that the core CFTR was detected at approximately 150 kD in both tissues, suggesting that the N-glycosylation pattern of CFTR may be tissue specific (Figure

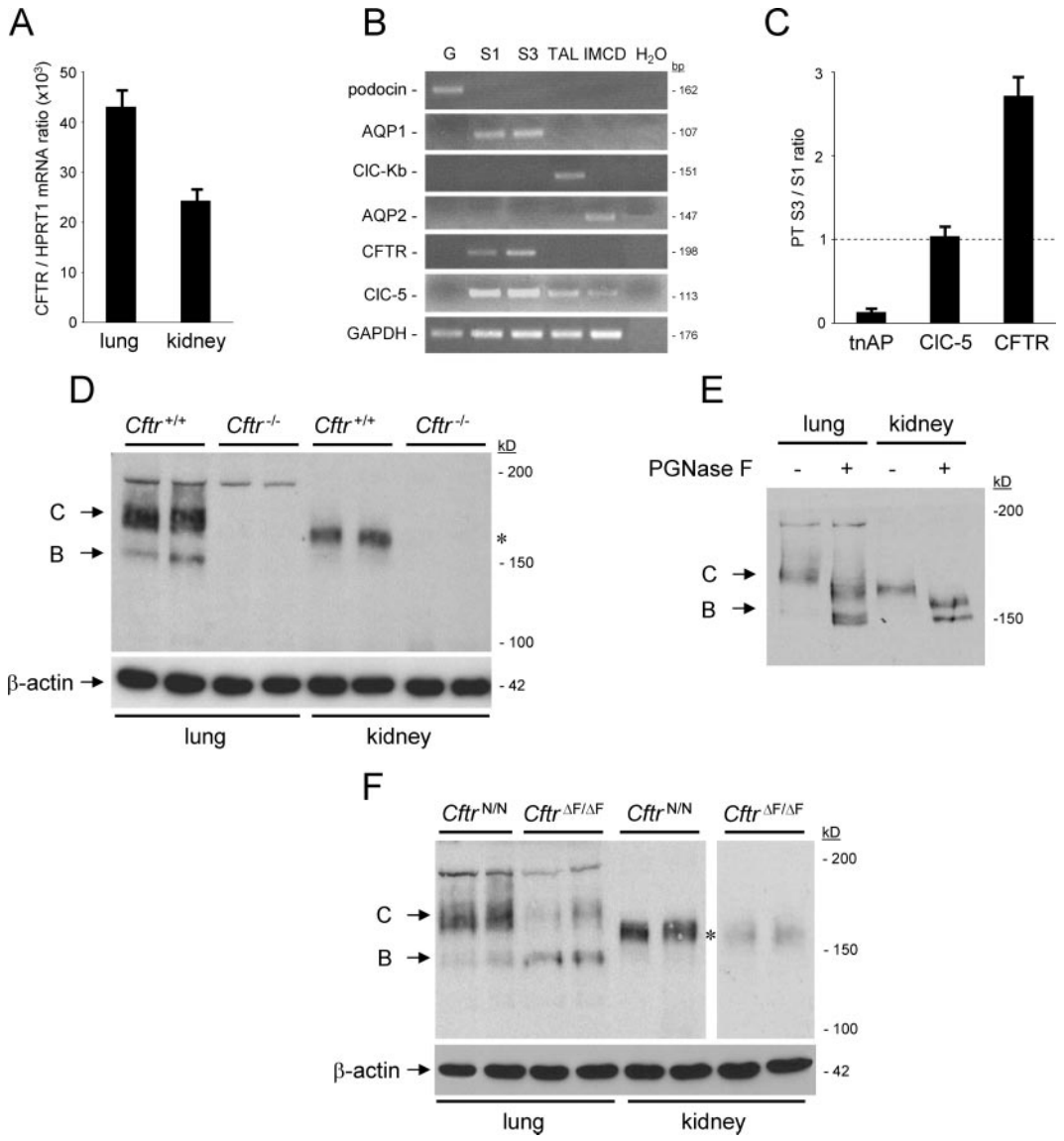

Figure 1. Expression of cystic fibrosis transmembrane conductance regulator (CFTR) in mouse kidney: mRNA and protein studies. (A) Comparative expression levels of CFTR mRNA in mouse lung and kidney by quantitative real-time reverse transcriptase–PCR (RT-PCR). The abundance of CFTR mRNA in kidney represents approximately 60% of that in lung, considered as the reference organ. Results are presented as ratios ($\times 10^3$) to the reporter gene *HPRT1* ($n = 4$ kidneys/lungs from four different mice). (B and C) Differential expression of CFTR in microdissected nephron segments. (B) Semiquantitative RT-PCR for segment-specific markers show that podocin is expressed in glomeruli, aquaporin-1 (AQP1) in proximal tubule (PT), ClC-Kb in thick ascending limbs (TAL), and AQP2 in inner medullary collecting ducts (IMCD). RT-PCR products (20 μl per lane) were size-fractionated on 1.5% agarose gel. (C) Real-time RT-PCR quantification demonstrates that the abundance of tissue-nonspecific alkaline phosphatase mRNA (tnAP) is approximately eight-fold greater in S1 than in S3 PT segments. ClC-5 mRNA is equivalent in S1 and S3 samples, whereas CFTR expression is approximately three-fold more abundant in S3 than in S1 segments ($n = 4$). (D) Representative immunoblotting for CFTR in lung and kidney from $Cftr^{+/+}$ and $Cftr^{-/-}$ mice. Membrane extracts (30 μg/lane) were run on 5% PAGE and transferred to nitrocellulose. The blot was probed with MD1314 anti-CFTR antibodies (1:500) and, after stripping, β-actin (1:10,000). In lung, both B (150 kD) and C bands (180 kD) are present, whereas, in kidney, CFTR is detected as a single large band at approximately 160 kD (asterisk at right). In both tissues, immunoreactive bands for CFTR are absent in $Cftr^{-/-}$ extracts. (E) Differential glycosylation of CFTR in mouse lung and kidney. Samples were incubated with (+) or without (−) N-glycosidase F for 90 min at 37°C. Treatment with N-glycosidase F induces a shift of CFTR bands to a lower molecular weight, indicating the presence of Asn-linked glycan chains in both lung and kidney samples, with CFTR core protein at approximately 150 kD. (F) Representative immunoblotting for ΔF508-CFTR in lung and kidney. In $Cftr^{\Delta F/\Delta F}$ lung, the fully glycosylated protein (C band) strongly decreases, whereas the B band increases. In the $Cftr^{\Delta F/\Delta F}$ kidney, there is a strong reduction in the CFTR immunodetection signal at 160 kD (*), requiring longer film exposure (60 min *versus* 1 min) for visualization.

1E). In contrast to various antibodies, the MD1314 antibodies used here did not detect any immunoreactive bands in tissue extracts from *Cftr*$^{-/-}$ mice (Figure 1D). The ΔF508 mutation is known to alter CFTR processing in lung (2). As shown in Figure 1F, the fully glycosylated C band was reduced markedly in *Cftr*$^{\Delta F/\Delta F}$ lung samples, whereas the B band was increased. In *Cftr*$^{\Delta F/\Delta F}$ kidney, a residual expression of ΔF508-CFTR was detected as a faint specific band at approximately 160 kD. These results validate the specificity of anti-CFTR antibodies that were used in this study and suggest a tissue-specific processing of CFTR. They also show that the defect of CFTR biosynthesis and/or stability that is caused by the ΔF508 mutation, previously documented in lung, also occurs in the kidney.

Segmental Localization and Subcellular Distribution of CFTR

Immunostaining that was performed on mouse kidney showed that CFTR is strongly detected at the corticomedullary junction, whereas the distribution of the PT multiligand receptor megalin includes both inner and outer cortices, as well as the outer stripe of the outer medulla (Figure 2, A and B). The co-localization of CFTR with AQP1 indicated that CFTR was detected in the apical area of PT cells. The signal was faint in S1 to S2 segments and stronger in the S3 segment of PT, close to the transition to the descending thin limb of Henle's loop (Figure 2, C, D, F, and G). The segmental location of the ΔF508-CFTR was similar to that of normal CFTR, including the apical region of the distal part of PT, although the immunoreactive signal was weaker than in control kidneys (Figure 2E). No specific signal for CFTR was detected in *Cftr*$^{-/-}$ kidneys (Figure 2H).

The subcellular distribution of CFTR in the kidney was investigated further by fractionation in Percoll gradients (Figure 3). These gradients resolved a low-density peak (fractions 2 through 5), including the early endosomal marker Rab5a; an intermediate density peak (fractions 7 through 9), including the brush border marker villin; and a bottom peak enriched in lysosomes (cathepsin D marker). The bulk of CFTR was detected in the endosomal fractions 3 through 4, where it co-localized with the vacuolar proton pump V-ATPase (E1 subunit) and ClC-5.

Altogether, these data support that, in mouse kidney, CFTR is particularly abundant in the S3 PT cells, with a subcellular distribution similar to ClC-5 and the V-ATPase in endosomes. Despite a weaker expression, the segmental location of the ΔF508-CFTR was preserved in mouse kidney.

Evaluation and Characterization of PT Apical Endocytosis in CF Mouse Models

Having established the segmental distribution of CFTR in the kidney, we investigated whether its disruption (*Cftr*$^{-/-}$ mice) or altered processing (*Cftr*$^{\Delta F/\Delta F}$ mice) influenced renal and PT function in mouse. Plasma and urine analyses revealed that the renal function was normal in both *Cftr*$^{-/-}$ and *Cftr*$^{\Delta F/\Delta F}$ mice (Table 1), with similar plasma bicarbonate and urine pH levels (data not shown). However, the significant increase in the urinary excretion of the LMW Clara cell protein (CC16, 16 kD) in *Cftr*$^{-/-}$ mice *versus* controls, contrasting with similar plasma

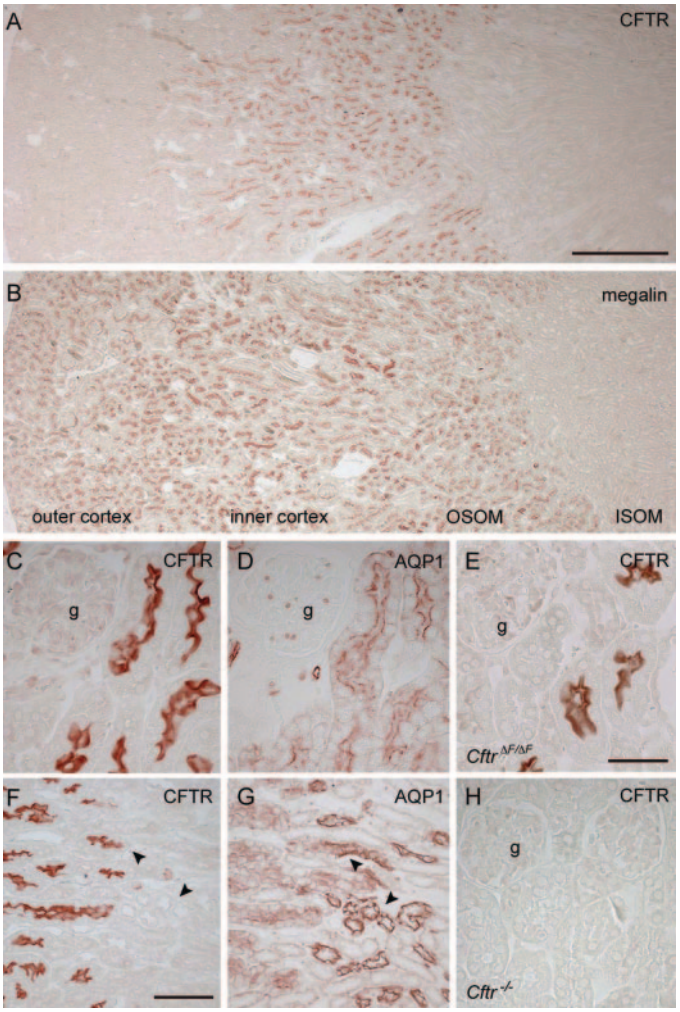

Figure 2. Localization of CFTR in mouse kidney. Immunoperoxidase labeling for CFTR (A, C, E, F, and H), megalin (B), and AQP1 (D and G) in mouse *Cftr*$^{+/+}$ (A through D, F, G), *Cftr*$^{\Delta F/\Delta F}$ (E), and *Cftr*$^{-/-}$ (H) kidneys. In control kidney, CFTR is detected preferentially at the corticomedullary junction, whereas megalin encompasses both inner and outer cortices and the outer stripe of the outer medulla (OSOM; compare A and B). The segmental co-localization of CFTR and AQP1 (C, D, F, and G) indicates that CFTR is particularly abundant in the apical area of the distal S3 segment of PT, just before the transition with the descending thin limb (F and G, arrowheads). No specific staining is observed in *Cftr*$^{-/-}$ kidney (H), whereas ΔF508-CFTR is detected with a lower intensity (requiring longer chromogenic reaction) in the S3 segment of PT (E). Bars = 500 μm in A and B; 100 μm in F and G); 50 μm in C, D, E, and H). g, glomerulus.

levels, suggested a deficient PT handling of LMW proteins in *Cftr*$^{-/-}$ mice. To test that hypothesis, we injected CF and control mice intravenously with ^{125}I-β_2-microglobulin, a LMW protein that is filtered freely by the glomerulus and taken up by receptor-mediated endocytosis in PT cells (25). After 7 min, renal uptake of ^{125}I-β_2-microglobulin was decreased significantly (up to 50%) in *Cftr*$^{-/-}$ mice *versus* their matched controls (Figure 4A). Liver uptake of ^{125}I-β_2-microglobulin, which was

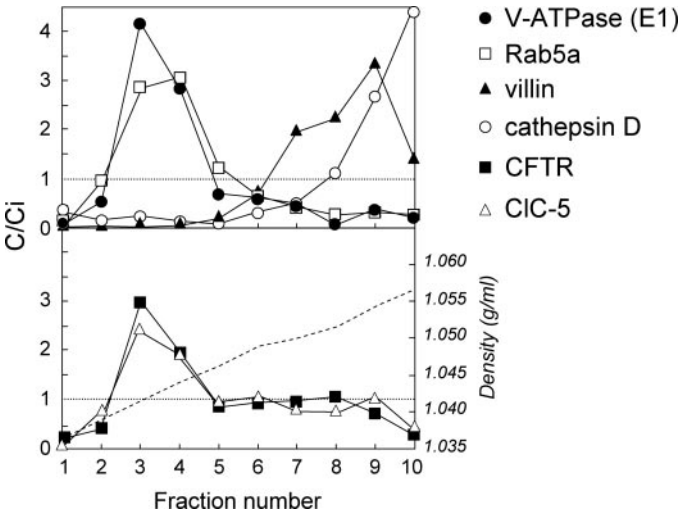

Figure 3. Subcellular distribution of CFTR in mouse kidney: Percoll gradient analyses. Percoll gradients of total mouse $Cftr^{+/+}$ kidney resolve a low-density peak (fractions 2 through 4), including the early endosomal maker Rab5a; an intermediate density peak (fractions 7 through 9), including the brush border component villin; and a bottom peak enriched in lysosomes (cathepsin D). Distributions after centrifugation are presented by comparison with the initial concentration as C/Ci (values >1 reflect organelle enrichment, and values <1 reflect organelle depletion). Typical densities are indicated by a broken line in the lower panel. CFTR co-distributes with ClC-5 and the vacuolar H^+-ATPase (E1 subunit) in endosomal fractions 3 through 4.

used as internal control because CFTR is not expressed in hepatocytes, was similar in both groups (data not shown). The $Cftr^{\Delta F/\Delta F}$ population showed an approximately 30% decrease of ^{125}I-β_2-microglobulin uptake, the phenotype heterogeneity probably reflecting the variable, residual expression of ΔF508-CFTR in kidney (Figure 4B). Densitometry analyses estimated a 10-fold decrease (ranging from 5 to 20% of $Cftr^{+/+}$ level) of CFTR abundance in $Cftr^{\Delta F/\Delta F}$ kidneys in comparison with controls. The renal phenotype of $Cftr^{-/-}$ mice was mild in comparison with $Clcn5^{Y/-}$ mice, characterized by a major defect (approximately 85%) in ^{125}I-β_2-microglobulin renal uptake (Figure 4A).

To assess the role of CFTR in the segmental reabsorption of LMW proteins in the PT, we correlated the distribution of CFTR (immunostaining) and ^{125}I-β_2-microglobulin (autoradiography) on adjacent serial sections (Figure 4C). These studies showed that ^{125}I-β_2-microglobulin uptake occurred mostly in S1 to S2 PT segments that expressed megalin and ClC-5, whereas only a residual reabsorption was observed in the S3 PT segments with high CFTR immunoreactivity (Figure 4C, arrowheads). We next evaluated the total content of endocytic actors (megalin, cubilin, and ClC-5) in CF *versus* control kidneys (Figure 5). No significant changes were observed in the kidneys from $Cftr^{\Delta F/\Delta F}$ mice (data not shown). In contrast, a specific decrease of cubilin expression was observed in $Cftr^{-/-}$ kidneys (Figure 5A), although no deficit was found at the mRNA level (data not shown). Immunofluorescence staining showed that the intensity of cubilin staining in $Cftr^{-/-}$ PT cells was markedly weaker at the corticomedullary junction (S3 PT segment) than in the outer cortex, whereas no differences were observed in $Cftr^{+/+}$ kidneys (Figure 5B). The differential immunoreactive pattern of cubilin in the $Cftr^{-/-}$ S3 PT cells was specific, because no similar modifications were observed for megalin (Figure 5B). Such cubilin defect was reflected further by the urinary loss of its ligand transferrin (76 kD) in the $Cftr^{-/-}$ mice (Figure 5C). To investigate further the biosynthesis and processing of cubilin, we performed deglycosylation assays in $Cftr^{-/-}$ *versus* $Cftr^{+/+}$ kidney samples, showing that cubilin correctly matured into its endoglycosidase H-resistant, N-glycosidase F-sensitive form in both groups (Figure 6A). In contrast, the abundance of cubilin in $Cftr^{-/-}$ mouse urine was increased significantly in comparison with controls, with no change of megalin urinary excretion levels (Figure 6B).

These data suggest that in $Cftr^{-/-}$ mice, the complete loss of CFTR induces a significant decrease in the membrane stability and increased urinary excretion of cubilin, leading to a defective apical receptor–mediated endocytosis in PT cells, with urinary loss of LMW ligands (β_2-microglobulin, CC16, and transferrin). This phenotype is observed less consistently in $Cftr^{\Delta F/\Delta F}$ mice, which may be explained by a variable residual expression and/or functionality of the mutated ΔF508-CFTR in the $Cftr^{\Delta F/\Delta F}$ kidneys (24,33).

Evaluation of PT Endocytosis in Patients with CF or Chronic Lung Inflammation

To substantiate the renal phenotype that was found in CF mouse models, we analyzed the urinary excretion of LMW proteins in a first series of stable patients with CF *versus* age- and gender-matched control subjects ($n = 30$ pairs). A second series of patients with chronic active asthma and their appropriate control subjects ($n = 25$ pairs) were investigated to rule out the potential interference of chronic lung inflammation with renal PT function. Figure 7 shows that, when normalized to the appropriate controls, there was a major, 30-fold increase in the transferrinuria, as well as a significant, two-fold increase in the urinary excretion of albumin, CC16, and β_2-microglobulin in patients with CF, whereas there were no significant changes in patients with asthma (Supplementary Table 2). No changes in the urinary concentration of calcium were observed. A multivariate model using stepwise regression showed that the four urinary protein ratios were associated significantly with CF, independent of gender, age, and previous treatment with aminosides, whereas no significant association existed with asthma. These data support that the PT dysfunction that was observed in the CF cohort likely is caused by CFTR dysfunction itself rather than a chronic state of lung inflammation.

Discussion

The spectrum of CF, which previously was considered as a respiratory and digestive disease associated with a rapidly fatal outcome, has broadened considerably in the past decade. The disease includes many milder cases, which are associated with a longer survival and a potential for developing complications in multiple organs (2,3). On the basis of recent insights into the

Table 1. Clinical and biological parameters in control and cystic fibrosis mouse models[a]

Genotype	Weight (g)	Plasma			Urine			
		Creatinine (mg/dl)	Urea (mg/dl)	CC16 (μg/L)	Diuresis (nl/min per g)	Urea (g/L)	Na^+ (mEq/L)	Ratio CC16/ Creatinine
$Cftr^{+/+}$ ($n = 5$)	28 ± 5	0.6 ± 0.1	19.1 ± 1.8	57.8 ± 6	26 ± 4	161.7 ± 16.1	280 ± 21	5 ± 2
$Cftr^{-/-}$ ($n = 5$)	27 ± 2	0.6 ± 0.1	17.8 ± 1.5	59.6 ± 4	24 ± 3	144.1 ± 5.2	270 ± 22	39 ± 13[b]
$Cftr^{N/N}$ ($n = 6$)	25 ± 1	0.7 ± 0.1	21.1 ± 0.9	53.9 ± 3	28 ± 2	159.2 ± 13.2	316 ± 19	17 ± 4
$Cftr^{\Delta F/\Delta F}$ ($n = 6$)	24 ± 1	0.6 ± 0.1	19.6 ± 1.2	52.1 ± 4	28 ± 3	142.7 ± 15.3	346 ± 16	18 ± 4

[a]Data are means ± SEM. Values were compared by nonparametric Mann-Whitney test. CC16, Clara cell 16-kD protein.
[b]$P < 0.05$.

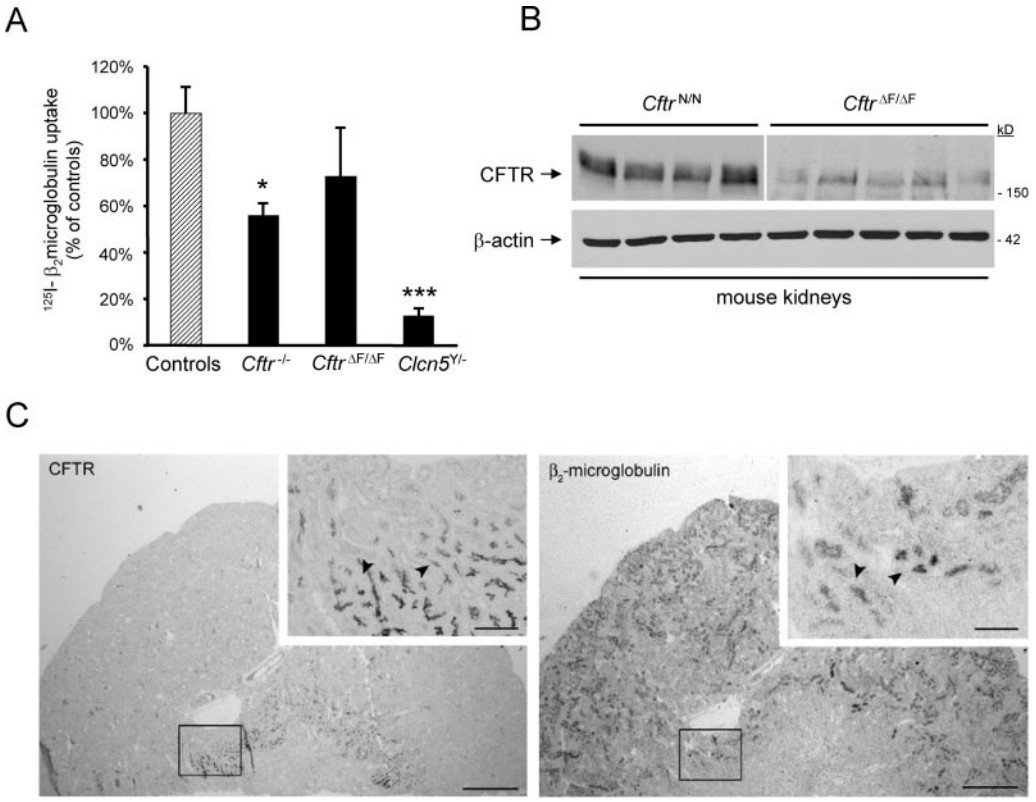

Figure 4. Investigation of PT apical endocytosis in CF and control kidneys. (A) Quantification of ^{125}I-β_2-microglobulin uptake in $Cftr^{-/-}$ and in $Cftr^{\Delta F/\Delta F}$ *versus* control kidneys. Seven minutes after intravenous injection, radioactivity was measured from bleached kidneys. Uptake of ^{125}I-β_2-microglobulin in the $Cftr^{-/-}$ kidneys is decreased significantly in comparison with age- and gender-matched kidneys (*$P < 0.05$); the decrease is less consistent in the ΔF508 population, characterized by a large phenotypic heterogeneity. The severe reduction of ^{125}I-β_2-microglobulin uptake in $Clcn5^{Y/-}$ kidneys (***$P < 0.001$) is indicated for comparison. The latter values were computed from reference (22). (B) Representative immunoblotting for ΔF508-CFTR in $Cftr^{\Delta F/\Delta F}$ kidneys. Membrane extracts from four and five individual $Cftr^{N/N}$ and $Cftr^{\Delta F/\Delta F}$ kidneys (40 μg/lane), respectively, were run on 5% PAGE and transferred to nitrocellulose. The blots were probed with MD1314 anti-CFTR antibodies (1:500) and β-actin (1:10,000), respectively. Densitometry showed that residual expression of ΔF508-CFTR averages 10-fold, with high individual variability between $Cftr^{\Delta F/\Delta F}$ kidney samples. (C) Comparative localization of CFTR and endocytosed ^{125}I-β_2-microglobulin (7 min) in mouse kidney. CFTR immunodetection and autoradiography were performed on serial kidney sections. CFTR is expressed preferentially in the inner cortex, whereas endocytosed ^{125}I-β_2-microglobulin is detected in both inner and outer cortices. The CFTR-positive tubules that are positive for ^{125}I-β_2-microglobulin (insets, arrowhead) provide a molecular explanation for the defect in receptor-mediated endocytosis. Bars = 500 μm; 100 μm (inset).

role of chloride transporters in the kidney (4,18), we analyzed the consequences of a functional loss of CFTR and showed it to be associated with an impaired cubilin-mediated endocytosis in renal PT cells, leading to LMW proteinuria in both mouse and human. Both CFTR and the renal chloride/proton exchanger ClC-5 preferentially associate with the endosomal marker

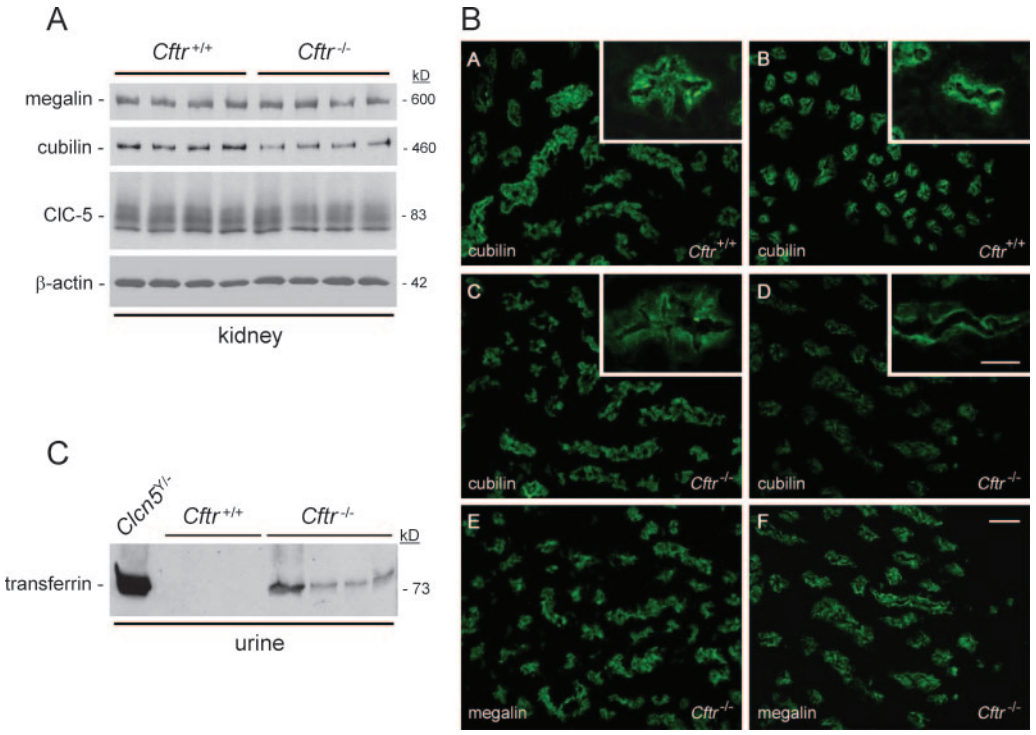

Figure 5. Total content of endocytic receptors and ClC-5 in $Cftr^{+/+}$ and $Cftr^{-/-}$ kidneys. (A) Representative immunoblotting for megalin, cubilin, and ClC-5 in $Cftr^{-/-}$ *versus* $Cftr^{+/+}$ kidneys. Membrane extracts (30 μg/lane) were run on 5% PAGE and transferred to nitrocellulose. The blots were probed with anti-megalin (1:20,000), anti-cubilin (1:10,000), or anti-ClC-5 (1:1000) antibodies and, after stripping, β-actin (1:10,000). Densitometry analyses were obtained from duplicate blots, after normalization to β-actin in each lane and comparison with $Cftr^{+/+}$ samples regarded as the 100% reference. In $Cftr^{-/-}$ extracts, the expression of megalin and ClC-5 is not modified, whereas cubilin abundance is reduced by approximately 50% ($^*P < 0.05$). (B) Immunofluorescence labeling for the multiligand receptors cubilin (A through D) and megalin (E and F) in $Cftr^{+/+}$ (A and B) and $Cftr^{-/-}$ (C through F) kidneys. Cubilin is detected in all PT segments of the outer cortex (A and C) and the corticomedullary junction of $Cftr^{+/+}$ and $Cftr^{-/-}$ kidneys. In $Cftr^{-/-}$ kidneys, the immunoreactive signal of cubilin in S3 PT (D) is weaker (insets) than in S1 through S2 segments (C), without changes in megalin abundance (E and F). Immunostaining experiments were performed strictly in parallel on two distinct $Cftr^{+/+}$ and $Cftr^{-/-}$ paired samples. Green fluorescence was visualized during 3 ms using the software IM50 (Zeiss, Zaventem, Belgium) through a Zeiss Axiovert S100 microscope equipped with an Axiocam camera. Bars = 50 μm; 20 μm (insets). (C) Urinary excretion of transferrin in $Cftr^{+/+}$ and $Cftr^{-/-}$ mice. Urine samples were loaded on 7.5% PAGE, blotted to nitrocellulose, and incubated with rabbit antibody anti-transferrin (1:1000). Loading volume was normalized to urine creatinine concentration; urine from $Clcn5^{Y/-}$ mouse was used as positive control (21). Transferrin, a specific ligand of cubilin, is detected in the urine from $Cftr^{-/-}$ mice but absent in the $Cftr^{+/+}$ samples.

Rab5a and the V-ATPase in PT cells. The striking contrast between the severe PT dysfunction that is associated with ClC-5 loss and the mild renal phenotype of CF probably reflects the distribution of these transporters in specialized segments of the PT.

Although the role of CFTR in exocrine epithelia, including trachea and small intestine, has been studied extensively (2,3), the issues of CFTR distribution, processing, and function in the kidney remain debated (4–9). In rat kidney, immunostaining for CFTR was shown at the apical surface of both proximal and distal tubules but was not detected in the outer medullary CD (5). In the human kidney, CFTR protein expression was found in the PT, thin limbs of Henle's loop, distal tubules, and collecting ducts (5–7). Our studies in mouse kidney (using antibodies of strict specificity) show that CFTR is expressed in the apical area of PT cells, with a maximal intensity in the S3 part of the PT. Furthermore, the electrophoretic mobility of N-glycosylated CFTR is slightly different in kidney *versus* lung, although CFTR core protein is detected at approximately 150 kD in both tissues. The established relationship between CFTR glycosylation and its stability/function at the plasma membrane (34) suggests that the distinct CFTR maturation in the kidney may reflect distinct trafficking/targeting and possibly different channel activity within tubular cells (35).

In parallel to its role in regulating chloride permeability across the apical membrane, CFTR also may facilitate the acidification of intracellular organelles along the endocytic pathway (15). Accordingly, an acidification defect was found in *trans*-Golgi and prelysosomal compartments in immortalized respiratory epithelial cells and nasal polyps from patients with CF (16). More recently, however, enhanced rather than decreased acidification was reported in endosomes of CF respiratory epithelial cells (17). Our fractionation data show that, in mouse kidney, CFTR co-distributes with ClC-5 and the V-ATPase in PT

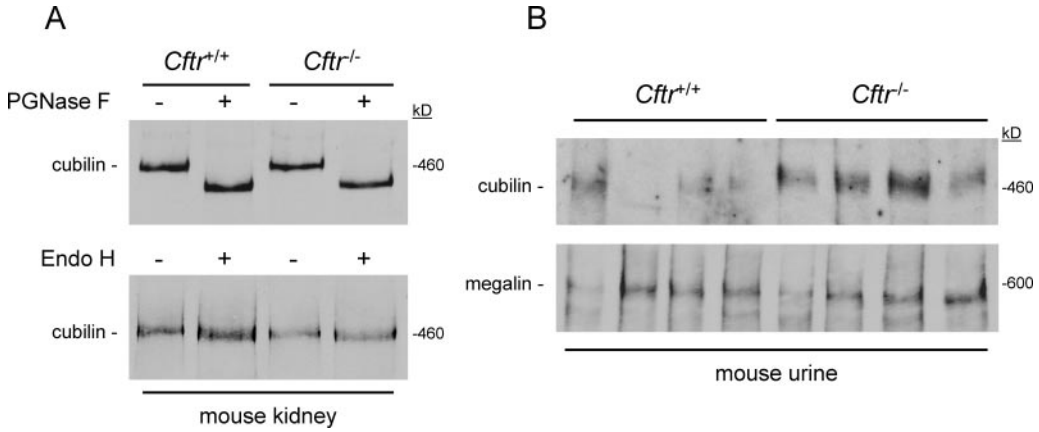

Figure 6. Processing of cubilin in *Cftr*$^{-/-}$ *versus Cftr*$^{+/+}$ kidneys. (A) Glycosylation status of cubilin in *Cftr*$^{-/-}$ *versus Cftr*$^{+/+}$ kidneys. Samples were incubated with (+) or without (−) N-glycosidase F for 90 min at 37°C or in endoglycosidase H (Endo H) overnight at 37°C. Treatment with N-glycosidase F induces a shift of cubilin immunoreactive band to a lower molecular weight, whereas no shift is observed after incubation with Endo H. The pattern is similar in both genotypes. (B) Excretion of cubilin in *Cftr*$^{-/-}$ *versus Cftr*$^{+/+}$ mouse urine. Urine samples were loaded on 5% PAGE, blotted to nitrocellulose, and incubated with antibody anti-cubilin (1:10,000). Loading volume was normalized to urine creatinine concentration. Cubilin abundance is increased significantly in the urine of *Cftr*$^{-/-}$ mice, whereas megalin is unchanged.

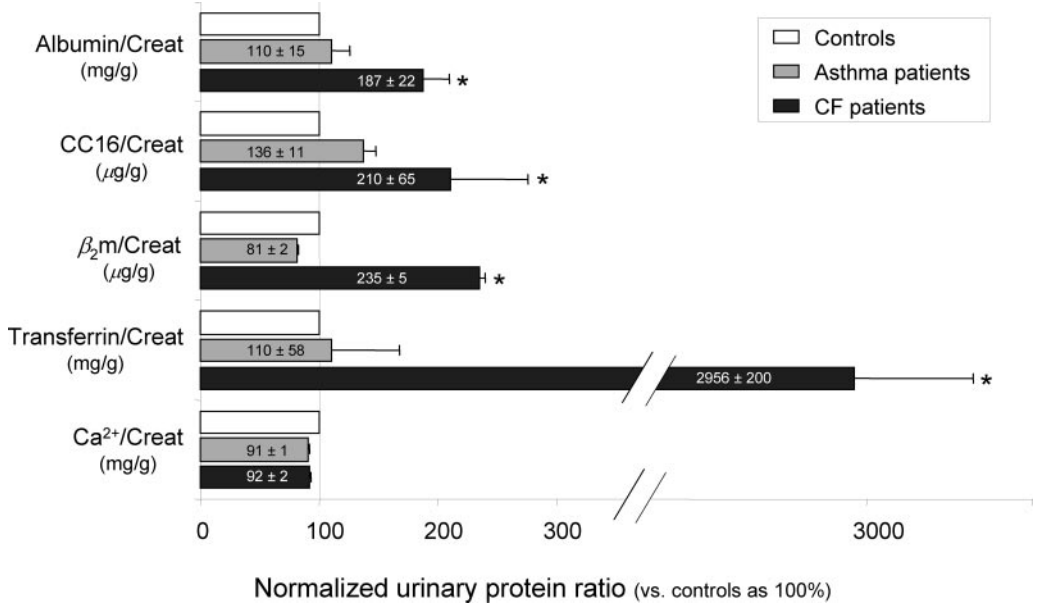

Figure 7. Low molecular weight proteinuria and calciuria in patients with CF or chronic lung inflammation. The urinary protein ratios for albumin, Clara cell protein (CC16), β_2-microglobulin (β_2m), and transferrin, as well as the calciuria, were investigated in a first series of patients with CF and age- and gender-matched control subjects ($n = 30$ pairs) and a second series of patients with active asthma (chronic lung inflammation) and their age- and gender-matched control subjects ($n = 25$ pairs). The geometric mean (±SEM) normalized to the appropriate control (taken as 100%) is given for each parameter. *$P < 0.05$.

endosomes, pointing to a possible involvement in apical endocytosis. The endocytic uptake of LMW proteins is mediated by the multiligand receptors megalin and cubilin, which are particularly expressed at the apical surface of cells that line the S1 to S2 segments of the PT (19). Recently, the vesicular chloride/proton exchanger ClC-5 has been involved clearly in renal endocytosis (20–22). Mutations of *CLCN5* gene that encodes ClC-5 cause Dent's disease, a tubulopathy that essentially is characterized by a generalized dysfunction of the PT associated with LMW proteinuria, hypercalciuria, and nephrolithiasis (22). Studies in *Clcn5*$^{Y/-}$ mice demonstrated that the loss of ClC-5 induces a defect in intracellular trafficking and membrane recycling in PT cells (20,21,25), confirming the crucial role of vesicular chloride transporters along the endocytic pathway. Likewise, the moderate but significant alteration of LMW protein handling that was observed in *Cftr*$^{-/-}$ mice and patients with CF suggests that CFTR may play a role in PT endocytosis.

In contrast to megalin, which is a member of the LDL recep-

tor family, cubilin is a multiligand receptor with little structural homology to known endocytic receptors and is characterized by the absence of transmembrane domain (36). Limited information is available about the regulators of cubilin targeting and processing in the PT. However, it was demonstrated recently that the apical targeting of cubilin depends on the correct glycosylation of its extracellular domains, as well as on reciprocal interactions with the transmembrane protein amnionless (37). Our data support that CFTR is more abundant in the S3 segment of the PT and present in endosomes. Its functional loss is associated with a selective decrease of cubilin expression in the S3 segment (Figure 5), reflected by the increased urinary excretion of cubilin ligands. Further investigations revealed that the lack of CFTR is not associated with changes in the biosynthesis of cubilin, as evidenced by similar mRNA levels (real-time PCR), similar glycosylation pattern (Figure 6), and similar bimodal distribution in subcellular fractions (data not shown). However, there was a significant increase in the urinary loss of cubilin in the $Cftr^{-/-}$ mice, contrasting with a lack of change for urinary megalin (Figure 6). Taken together, these data suggest that the lack of CFTR in the S3 segment is reflected by an instability of cubilin in the apical membrane, leading to its accelerated shedding in the urine. Although the lack of suitable reagents prevented investigation of the specific role of amnionless in the process, it is tempting to hypothesize that such cubilin instability could be due to the improper processing or trafficking of one of its partners in relation with the lack of CFTR in that nephron segment (15,17). Of note, a decrease in cubilin has been observed in the small intestine of the CFTR null ($Cftr^{tm1UNC}$) mouse, which may explain a reduced vitamin B_{12} absorption in patients with CF (38). Moreover, preliminary data showing a lower renal uptake of aminoglycosides in CF mice in comparison with controls (F.J. *et al.*, unpublished observations) suggest that the defect in receptor-mediated endocytosis reported here also may explain why the renal clearance of aminosides is enhanced in patients with CF (13,39).

The patients with CF examined here, all harboring at least one ΔF508 mutation, showed a mild LMW proteinuria *versus* healthy control subjects, whereas no significant changes were observed in patients with chronic lung inflammation that was caused by active asthma. Of particular interest is the major, 30-fold increase in transferrinuria in the patients with CF, reflecting the cubilin defect and transferrinuria evidenced in the $Cftr^{-/-}$ mice. These findings may be clinically relevant, because LMW proteinuria can trigger tubulointerstitial injury (19,36). Moreover, the increased loss of transferrin in the urine could participate in the iron deficiency and lower circulating transferrin levels that are common in patients with CF (40,41). The endocytic defect was less consistent in the $Cftr^{\Delta F/\Delta F}$ mice, which showed either unchanged or increased urinary excretion of LMW proteins. The mutant ΔF508-CFTR shows defective glycosylation and traffic (2,3). However, ΔF508-CFTR can function as a cAMP-regulated chloride channel, both in the plasma membrane and intracellularly (27). Previous studies demonstrated a residual chloride permeability in intestine and gallbladder of the $Cftr^{\Delta F/\Delta F}$ mice used here (24), and the electrolyte and water handling is preserved in the PT of $Cftr^{tm2cam}$ ΔF508 mice (42). We documented an approximately two-fold reduction in ΔF508-CFTR mRNA abundance in $Cftr^{\Delta F/\Delta F}$ *versus* $Cftr^{N/N}$ kidneys (data not shown) and a large individual variability (ranging from 5 to 20% of the control level) in the residual expression of ΔF508-CFTR protein. The expression of ΔF508-CFTR in human is strikingly tissue specific, suggesting that the variable severity of CF in various organs reflects heterogeneity of residual expression (33,43). Taken together, these data suggest that, in mouse kidney, the ΔF508-CFTR is processed variably into its mature form, reaching the plasma membrane and ensuring correct function in some $Cftr^{\Delta F/\Delta F}$ mice.

Several explanations may account for the milder renal phenotype that is observed in $Cftr^{-/-}$ mice and patients with CF in comparison with *Clcn5* KO mice and patients with Dent's disease (20–22). First, it could reflect the more distal distribution of CFTR as compared with ClC-5 along the PT. Indeed, although ClC-5 is distributed evenly in the S1 to S3 parts of the PT, CFTR seems to be most abundant in the S3 segment of the PT, which displays lower endocytic activity (44). Second, CFTR functions as a cAMP-regulated, ATP-dependent chloride channel, whereas the flux of chloride through ClC-5 depends constitutively on transmembrane Cl^- and H^+ concentration gradient, together with the membrane voltage (18). The number of active CFTR channels also is known to be regulated by cAMP-dependent vesicle trafficking, as well as by correct glycosylation (2,35). Third, the discrete nature of renal manifestations in CF might be due to tissue-specific protective mechanisms, such as the occurrence of functional CFTR splice variants (7,8), or alternative pathways for chloride (4). For instance, a Ca^{2+}-activated Cl^- channel is upregulated in the nasal mucosa of $Cftr^{tm1UNC}$ mice (45). Although ClC-5 might represent a CFTR surrogate, a comparative analysis that was performed on $Cftr^{-/-}$ *versus* $Cftr^{+/+}$ kidneys did not show any changes in ClC-5 expression (Figure 5).

Conclusion

The functional loss of CFTR is associated with a moderate but significant defect in LMW protein handling in mouse and human, supporting a role of CFTR in the cubilin-mediated endocytic pathway in renal PT cells. These data give new insights into the tissue-specific processing of wild-type and mutant CFTR and the pathophysiology of chloride transporters in the kidney. The urinary loss of LMW proteins, including transferrin, should be integrated in the pathophysiology of multisystemic complications that increasingly are observed in patients with CF.

Acknowledgments

This work was supported by the Belgian agencies Fonds National de la Recherche Scientifique (FNRS) and Fonds de la Recherche Scientifique Médicale, the Foundation Alphonse et Jean Forton, Concerted Research Actions, Inter-University Attraction Poles, the Association Belge de Lutte contre la Mucoviscidose, a grant from Amgen, and the EuReGene integrated project of the European Community (FP6). F.J. is a Research Fellow of the FNRS.

We are grateful to R. Beauwens, X. Dumont, V. Godding, S.E. Guggino, W.B. Guggino, P. Nguyen, C. Pilette, and P. Verroust for helpful discus-

sions and material and to Y. Cnops, H. Debaix, M. Leruth, T. Lac, P. Van der Smissen, and L. Wenderickx for excellent technical assistance.

Disclosures

None.

References

1. Riordan JR, Rommens JM, Kerem B, Alon N, Rozmahel R, Grzelczak Z, Zielenski J, Lok S, Plavsic N, Chou JL, *et al.*: Identification of the cystic fibrosis gene: Cloning and characterization of complementary DNA. *Science* 245: 1066–1073, 1989
2. Sheppard DN, Welsh MJ: Structure and function of the CFTR chloride channel. *Physiol Rev* 79[Suppl 1]: S23–S45, 1999
3. Rowe SM, Miller S, Sorscher EJ: Cystic fibrosis. *N Engl J Med* 352: 1992–2001, 2005
4. Devuyst O, Guggino WB: Chloride channels in the kidney: Lessons learned from knockout animals. *Am J Physiol Renal Physiol* 283: F1176–F1191, 2002
5. Crawford I, Maloney PC, Zeitlin PL, Guggino WB, Hyde SC, Turley H, Gatter KC, Harris A, Higgins CF: Immunocytochemical localization of the cystic fibrosis gene product CFTR. *Proc Natl Acad Sci U S A* 88: 9262–9266, 1991
6. Devuyst O, Burrow CR, Schwiebert EM, Guggino WB, Wilson PD: Developmental regulation of CFTR expression during human nephrogenesis. *Am J Physiol* 27: F723–F735, 1996
7. Morales MM, Carroll TP, Morita T, Schwiebert EM, Devuyst O, Wilson PD, Lopes AG, Stanton BA, Dietz HC, Cutting GR, Guggino WB: Both the wild type and a functional isoform of CFTR are expressed in kidney. *Am J Physiol* 270: F1038–F1048, 1996
8. Huber S, Braun G, Burger-Kentischer A, Reinhart B, Luckow B, Horster M: CFTR mRNA and its truncated splice variant (TRN-CFTR) are differentially expressed during collecting duct ontogeny. *FEBS Lett* 423: 362–366, 1998
9. Stanton BA: Cystic fibrosis transmembrane conductance regulator (CFTR) and renal function. *Wien Klin Wochenschr* 109: 457–464, 1997
10. Katz SM, Krueger LJ, Falkner B: Microscopic nephrocalcinosis in cystic fibrosis. *N Engl J Med* 319: 263–266, 1988
11. Gibney EM, Goldfarb DS: The association of nephrolithiasis with cystic fibrosis. *Am J Kidney Dis* 42: 1–11, 2003
12. Berg U, Kusoffsky E, Strandvik B: Renal function in cystic fibrosis with special reference to the renal sodium handling. *Acta Paediatr Scand* 71: 833–838, 1982
13. Samaniego-Picota MD, Whelton A: Aminoglycosides-induced nephrotoxicity in cystic fibrosis: A case presentation and review of the literature. *Am J Ther* 3: 248–257, 1996
14. Crawford IT, Maloney PC: Identification of cystic fibrosis transmembrane conductance regulator in renal endosomes. *Methods Enzymol* 292: 652–663, 1998
15. Bradbury NA: Intracellular CFTR: Localization and function. *Physiol Rev* 79[Suppl 1]: S175–S191, 1999
16. Barasch J, Kiss B, Prince A, Saiman L, Gruenert D, al-Awqati Q: Defective acidification of intracellular organelles in cystic fibrosis. *Nature* 352: 70–73, 1991
17. Poschet JF, Skidmore J, Boucher JC, Firoved AM, Van Dyke RW, Deretic V: Hyperacidification of cellubrevin endocytic compartments and defective endosomal recycling in cystic fibrosis respiratory epithelial cells. *J Biol Chem* 277: 13959–13965, 2002
18. Jentsch TJ, Maritzen T, Zdebik AA: Chloride channel diseases resulting from impaired transepithelial transport or vesicular function. *J Clin Invest* 115: 2039–2046, 2005
19. Christensen EI, Birn H: Megalin and cubilin: Multifunctional endocytic receptors. *Nat Rev Mol Cell Biol* 3: 256–266, 2002
20. Piwon N, Gunther W, Schwake M, Bosl MR, Jentsch TJ: ClC-5 Cl−-channel disruption impairs endocytosis in a mouse model for Dent's disease. *Nature* 408: 369–373, 2000
21. Wang SS, Devuyst O, Courtoy PJ, Wang XT, Wang H, Wang Y, Thakker RV, Guggino S, Guggino WB: Mice lacking renal chloride channel, CLC-5, are a model for Dent's disease, a nephrolithiasis disorder associated with defective receptor-mediated endocytosis. *Hum Mol Genet* 9: 2937–2945, 2000
22. Lloyd SE, Pearce SH, Fisher SE, Steinmeyer K, Schwappach B, Scheinman SJ, Harding B, Bolino A, Devoto M, Goodyer P, Rigden SP, Wrong O, Jentsch TJ, Craig IW, Thakker RV: A common molecular basis for three inherited kidney stone diseases. *Nature* 379: 445–449, 1996
23. Ratcliff R, Evans MJ, Cuthbert AW, MacVinish LJ, Foster D, Anderson JR, Colledge WH: Production of a severe cystic fibrosis mutation in mice by gene targeting. *Nat Genet* 4: 35–41, 1993
24. van Doorninck JH, French PJ, Verbeek E, Peters RH, Morreau H, Bijman J, Scholte BJ: A mouse model for the cystic fibrosis delta F508 mutation. *EMBO J* 14: 4403–4411, 1995
25. Christensen EI, Devuyst O, Dom G, Nielsen R, Van der Smissen P, Verroust P, Leruth M, Guggino WB, Courtoy PJ: Loss of chloride channel, ClC-5, impairs endocytosis by defective trafficking of megalin and cubilin in kidney proximal tubules. *Proc Natl Acad Sci U S A* 100: 8472–8477, 2003
26. Wagner CA, Lukewille U, Valles P, Breton S, Brown D, Giebisch GH, Geibel JP: A rapid enzymatic method for the isolation of defined kidney tubule fragments from mouse. *Pflugers Arch* 446: 623–632, 2003
27. French PJ, van Doorninck JH, Peters RH, Verbeek E, Ameen NA, Marino CR, de Jonge HR, Bijman J, Scholte BJ: A delta F508 mutation in mouse cystic fibrosis transmembrane conductance regulator results in a temperature-sensitive processing defect in vivo. *J Clin Invest* 98: 1304–1312, 1996
28. Jouret F, Igarashi T, Gofflot F, Wilson PD, Karet FE, Thakker RV, Devuyst O: Comparative ontogeny, processing, and segmental distribution of the renal chloride channel, ClC-5. *Kidney Int* 65: 198–208, 2004
29. Jouret F, Auzanneau C, Debaix H, Sun Wada GH, Pretto C, Marbaix E, Karet FE, Courtoy PJ, Devuyst O: Ubiquitous and kidney-specific subunits of the vacuolar H+-ATPase are differentially expressed during nephrogenesis. *J Am Soc Nephrol* 16: 3235–3246, 2005
30. Bernard A, Chia KS, Lauwerys R: Latex immunoassay of transferrin in urine. *J Immunol Methods* 144: 49–55, 1991
31. Bernard A, Thielemans N, Lauwerys R, Van Lierde M: Selective increase in the urinary excretion of protein 1 (Clara cell protein) and other low molecular weight proteins during normal pregnancy. *Scand J Clin Lab Invest* 52: 871–878, 1992
32. Nouwen EJ, De Broe ME: Human intestinal versus tissue-

nonspecific alkaline phosphatase as complementary urinary markers for the proximal tubule. *Kidney Int Suppl* 47: S43–S51, 1994
33. Kalin N, Claass A, Sommer M, Puchelle E, Tummler B: DeltaF508 CFTR protein expression in tissues from patients with cystic fibrosis. *J Clin Invest* 103: 1379–1389, 1999
34. Denning GM, Anderson MP, Amara JF, Marshall J, Smith AE, Welsh MJ: Processing of mutant cystic fibrosis transmembrane conductance regulator is temperature sensitive. *Nature* 358: 761–764, 1992
35. O'Riordan CR, Lachapelle AL, Marshall J, Higgins EA, Cheng AH: Characterization of the oligosaccharide structures associated with the cystic fibrosis transmembrane conductance regulator. *Glycobiology* 10: 1225–1233, 2000
36. Birn H, Christensen EI: Renal albumin absorption in physiology and pathology. *Kidney Int* 69: 440–449, 2006
37. Coudroy G, Gburek J, Kozyraki R, Madsen M, Trugnan G, Moestrup SK, Verroust PJ, Maurice M: Contribution of cubilin and amnionless to processing and membrane targeting of cubilin-amnionless complex. *J Am Soc Nephrol* 16: 2330–2337, 2005
38. Norkina O, Kaur S, Ziemer D, De Lisle RC: Inflammation of the cystic fibrosis mouse small intestine. *Am J Physiol Gastrointest Liver Physiol* 286: G1032–G1041, 2004
39. Schmitz C, Hilpert J, Jacobsen C, Boensch C, Christensen EI, Luft FC, Willnow TE: Megalin deficiency offers protection from renal aminoglycosides accumulation. *J Biol Chem* 277: 618–622, 2002
40. Pond MN, Morton AM, Conway SP: Functional iron deficiency in adults with cystic fibrosis. *Respir Med* 90: 409–413, 1996
41. O'Connor TM, McGrath DS, Short C, O'Donnel MJ, Sheehy M, Bredin CP: Subclinical anemia of chronic disease in adult patients with cystic fibrosis. *J Cyst Fibros* 1: 31–34, 2002
42. Kibble JD, Balloch KJ, Neal AM, Hill C, White S, Robson L, Green R, Taylor CJ: Renal proximal tubule function is preserved in Cftr(tm2cam) deltaF508 cystic fibrosis mice. *J Physiol* 532: 449–457, 2001
43. Persu A, Devuyst O, Lannoy N, Materne R, Brosnahan G, Gabow PA, Pirson Y, Verellen-Dumoulin C: CF gene and cystic fibrosis transmembrane conductance regulator expression in autosomal dominant polycystic kidney disease. *J Am Soc Nephrol* 11: 2285–2296, 2000
44. Mori K, Lee HT, Rapoport D, Drexler IR, Foster K, Yang J, Schmidt-Ott KM, Chen X, Li JY, Weiss S, Mishra J, Cheema FH, Markowitz G, Suganami T, Sawai K, Mukoyama M, Kunis C, D'Agati V, Devarajan P, Barasch J: Endocytic delivery of lipocalin-siderophore-iron complex rescues the kidney from ischemia-reperfusion injury. *J Clin Invest* 115: 610–621, 2005
45. Grubb BR, Vick RN, Boucher RC: Hyperabsorption of Na+ and raised Ca++-mediated Cl− secretion in nasal epithelia of CF mice. *Am J Physiol Cell Physiol* 266: C1478–C1483, 1994

Supplemental information for this article is available online at http://www.jasn.org/.